Fibre behaviour in the spunbonding process. Part I: Characterisation of air flow and fibre motion in the diffuser

Journal:	*Part C: Journal of Mechanical Engineering Science*
Manuscript ID:	JMES-15-0238.R1
Manuscript Type:	Original article
Date Submitted by the Author:	20-Jul-2015
Complete List of Authors:	Battocchio, Francesco; University of Cambridge, Engineering Sutcliffe, Michael; University of Cambridge
Keywords:	Applied Mechanics, Dynamics, Polymers, Textile Technology, Turbulence
Abstract:	The random fibre oscillatory behaviour induced by turbulence in the diffuser of an industrial spun-bonding rig is measured experimentally. The turbulent air flow is firstly characterised by constant temperature hot-wire anemometry: averaged flow quantities, such as the mean velocity and the turbulent kinetic energy, as well as time dependent quantities, such as the integral time and the energy spectrum, are measured. The influence of the turbulent flow on the dynamics of a nylon fibre of diameter 200 μm and a spun-bonding fibre of diameter 18 μm in the diffuser is then investigated by extracting the transverse displacement from images acquired by a digital camera.

Journal Title
XX(X):1–8

DOI: 10.1177/ToBeAssigned
www.sagepub.com/
SAGE

Fibre behaviour in the spunbonding process. Part I: Characterisation of air flow and fibre motion

Francesco Battocchio[1], M. P. F. Sutcliffe[1] and F. Teschner[2]

Abstract

The random fibre oscillatory behaviour induced by turbulence in the diffuser of an industrial spun-bonding rig is measured experimentally. The turbulent air flow is firstly characterised by constant temperature hot-wire anemometry: averaged flow quantities, such as the mean velocity and the turbulent kinetic energy, as well as time dependent quantities, such as the integral time and the energy spectrum, are measured. The influence of the turbulent flow on the dynamics of a nylon filament of diameter 200 μm and a spun-bonding fibre of diameter 18 μm is then investigated by extracting the transverse displacement from images acquired by a digital camera.

Keywords

Nonwovens, spunbonding, turbulence, hot-wire anemometry, fibre dynamics, image processing

Introduction

Overview

The spunbonding process is a widespread method for the production of nonwoven materials in which thousands of fibres are firstly spun by an accelerated air flow, then randomly oscillated by a turbulent air flow in a diffuser, and finally deposited as a web on to a conveyor belt[1;2]. Fibre extrusion is enhanced in a contraction where a primary air stream is accelerated to help to attenuate the fibres by skin friction drag[3], from a diameter of about 200 microns, as the filaments leave the spinneret, to the final diameter in the range 20-70 microns. The air flow is also used to solidify the fibres during the attenuation process, as opposed to the meltblowing process in which fibres are not completely solidified when they reach the collector. After the contraction, fibres enter a diffuser which is fed both by the main air stream and by a secondary air stream, which is injected at the junction between the contraction and the diffuser. This secondary air enhances the intensity of turbulence in the diffuser and promotes random fibre oscillation before deposition. Such a step is fundamental for obtaining a more uniform fibre orientation in the corresponding web that forms on the collecting conveyor belt.

In spite of the lack of studies on fibre deposition, it is known from the pioneering work undertaken by Hearle[4–6] that a thread deposited on to a moving belt assumes the shape of a modified cycloid whose pitch increases by decreasing the fibre-belt velocity ratio. This mechanism results in a preferential fibre orientation in the forming web along the machine direction, i. e. the direction of the belt motion. In the spunbonding process the random drag force resulting from the interaction between the fibres and the turbulent flow in the diffuser is used to increase the isotropy of the fibre orientation during deposition. However, it is known that if the level of turbulence is too high, then the areal density of the fibre web becomes progressively less uniform, and properties such as strength, filtration and appearance are easily compromised. A comprehensive study of the fibre web formation requires a model of the details of the fibre laydown. However, this cannot be done until the fibre-flow interaction that takes place in the diffuser is fully understood. In particular it is crucial to know the amplitude of fibre oscillation and to find how the air flow in the diffuser influences the fibre motion before the fibres are deposited on the conveyor belt.

Air flow and fibre motion in the spunbonding diffuser

The literature of nonwovens contains extensive modelling and experimental work about fibre formation, but this typically neglects the influence of turbulence on the dynamics of the fibre[7–9]. Still a robust study that explains how the air flow in the diffuser influences the fibre motion, and in turn the web development, is missing. A stochastic model for fibre motion in turbulent air flows is presented in[10], where the turbulent air flow in the diffuser of an industrial spunbonding plant was obtained by computational fluid dynamics (CFD) using a standard $k-\varepsilon$ model. Turbulence models used in CFD are strictly valid only for steady and fully developed turbulent flows, whereas it is unlikely that such a condition holds in the spunbonding diffuser due to the adverse pressure gradient[11]. Therefore, an accurate characterisation of the fibre-air flow interaction can be obtained only if the air flow and the fibre motion are

[1]Department of Engineering, University of Cambridge,UK
[2]Fitesa GmbH, Germany

Corresponding author:
Francesco Battocchio, Department of Engineering, University of Cambridge, Trumpigton Street, Cambridge, CB2 1PZ, UK.
Email: francesco.battocchio@gmail.com

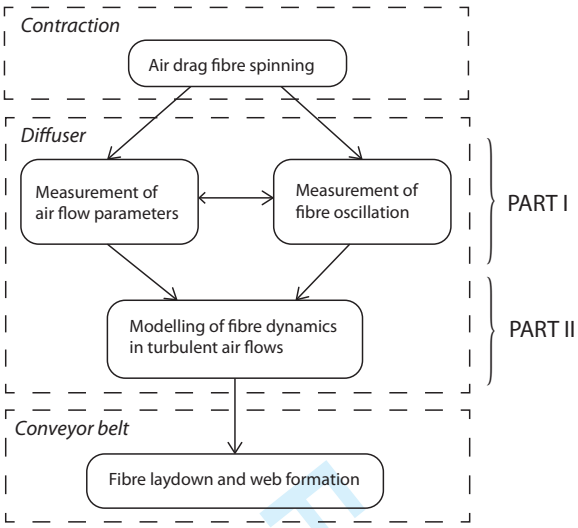

Figure 1. Outline of the paper and its contribution in the modelling of the spun-bonding process.

measured experimentally.

The motion and vibration of a fibre has been measured for the meltblowing process by using laser Doppler velocimetry (LDV)[12] and high-speed photography[7;13]. However, at present there are no available data for the air flow and the fibre motion in the spunbonding diffuser. We believe that this limitation is due mainly to two reasons. Firstly, an industrial process such as spunbonding cannot be easily reproduced in a laboratory environment due to the complexity of the rig. Besides, the process involves the production of thousands of fibres that move and entangle together, which prevents focusing on the interaction between the flow and the individual fibres. Finally, the measurement of fibre motion is more complex compared to meltblowing, since in spunbonding fibres are confined within the diffuser walls.

Figure 1 shows the contribution of our study on the analysis of the fibre behaviour in turbulent air flows, which is a necessary step for understanding the web formation in the spunbonding process and thereby improve the quality of nonwovens. The dynamics of fibre spinning has already been studied by other authors, as mentioned above, while here we focus on the fibre behaviour in the diffuser which is a prerequisite to predict the fibre laydown and the random web formation. In this paper, Part I, we measure the turbulent air flow in the diffuser of an industrial spunbonding rig by hot-wire anemometry. Then, under the same flow conditions, we measure the displacement of a single fibre and a single filament through the diffuser walls by digital image analysis. This allows us to identify the air flow parameters that influence the fibre motion, and to characterise the amplitude of fibre motion under the turbulent air flow in the diffuser. In the companion paper, Part II, we present a mathematical model for the fibre motion in turbulent air flows, that allows us to extend this investigation to different turbulent flow regimes, and to understand how the individual model parameters influence the fibre motion before laydown.

Characterisation of the diffuser air flow

Turbulence is defined as the chaotic motion of a fluid flow, unlike the laminar regime where the particles follow streamlines that are aligned with the mean flow direction. A turbulent flow is composed of interacting vortices that are stretched and twisted by the mean flow[14]. As a result, a turbulent velocity field varies in time and space in a random and unpredictable way.

In a laminar pipe flow, the velocity of the particles, sufficiently far from the wall, is uniform and constant in time. On the other hand, in a turbulent pipe flow the velocity is neither constant nor uniform. If $\overline{U}(\mathbf{x})$ is the time-averaged flow velocity directed in the stream-wise direction, and $u'(\mathbf{x},t)$ is the fluctuating velocity related to the vortex motion, the velocity of a turbulent flow is expressed as

$$U(\mathbf{x},t) = \overline{U}(\mathbf{x}) + u'(\mathbf{x},t) \tag{1}$$

In Equation 1 u' is a random signal with normal distribution and zero mean, and can be assumed locally isotropic in space. The magnitude of turbulence is evaluated through the dimensionless turbulence intensity

$$Tu = \frac{u}{U} \tag{2}$$

where u is the root mean square (rms) fluctuating velocity, and U is the mean air flow velocity.

This section presents the characterisation of the air flow in the diffuser in terms of mean velocity, turbulence intensity, and turbulence energy spectrum from air flow data measured by hot-wire anemometry.

Experimental equipment and procedure

Figure 2 shows a schematic of the diffuser and the reference system that will used to describe the air velocity fields. Here, x is the stream-wise direction, while y is the transverse direction along which air velocity profiles were acquired. The diffuser has a rectangular cross-section, with total length of 1 m, depth of 136 mm, and total divergence angle $\theta = 2°$. The primary air stream is injected from the contraction, while the secondary air stream is sucked in at the junction between the contraction and the diffuser from the still air into the system by the Venturi effect.

In the diffuser, the decrease in the air velocity gives rise to an adverse gradient of pressure that can lead to phenomena of instability, such as flow separation and backflow[15], that develop typically in the region near to the wall for large divergence angles and aspect ratios. In our rig the divergence angle is small enough to prevent flow separation[15], but the flow instability is such that the air flow is best characterized by an experimental technique rather than by computational simulations.

The air velocity in the diffuser was measured by Constant Temperature Hot-Wire Anemometry (CTHWA)[16], a technique that allows the measurement of the instantaneous velocity fluctuations. CTHWA is based on the convective heat transfer to the surrounding flow from a hot-wire probe, kept at constant temperature by the anemometer. Any variation in the flow velocity changes the transferred heat and, in turn, the voltage required to maintain the hot-wire at the working temperature. The velocity history of the flow

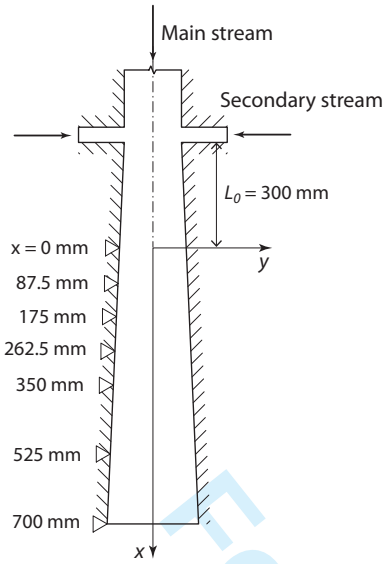

Figure 2. Schematic of the diffuser with the measurement sections.

is then measured from the instantaneous voltage applied to the hot-wire, through a calibration function.

Due to the increasing cross-section, the mean air flow velocity decreases downstream in the diffuser leading to a broad range of velocities from the inlet to the outlet of the diffuser. When a broad velocity range is to be measured, the best accuracy for the velocity data is achieved using a 4th order polynomial calibration function [17]

$$U(E) = C_0 + C_1 E + C_2 E^2 + C_3 E^3 + C_4 E^4 \qquad (3)$$

where E is the voltage measured by the hot-wire anemometer, and U is the instantaneous air flow velocity. The hot-wire probe was calibrated in a wind tunnel over the velocity range $0 - 30$ m/s, and the coefficients $C_0, \ldots, C_4$ were calculated by fitting Equation 3 to the velocities measured through a Pitot tube.

It is expected that the interaction between primary and secondary air streams leads to a complex air flow at the top of the diffuser. However, it is also expected that, because of the small divergence angle and the high aspect ratio, the mean air flow velocity will be aligned with the diffuser axis sufficiently downstream of the secondary air inlet. Therefore, hot-wire anemometry measurements were undertaken using a Single Normal (SN) probe which allows measurement of only one component of the flow velocity. Velocity data were acquired starting from a position $L_0 = 300$ mm downstream of the secondary air stream inlet, in order to guarantee the unidirectionality of the flow (see Figure 2). The movement of the probe was provided by a transverse system similar to that showed in [11] composed of a lead screw with pitch 1 mm, and fixed to the end of the diffuser. In this configuration the probe support is inserted into the diffuser from the outlet section, which has the advantage that measurements can be undertaken without any modification of the rig.

Air velocity measurements were executed using a DANTEC 54T30 *miniCTA* single channel hot-wire anemometer equipped with a 55P16 single normal probe. The voltage output from the anemometer was acquired using the external DAQ board USB-6009 from National Instruments, with voltage range $\pm$ 10 V, resolution of 14 bits, and maximum sampling rate of 48 kS/s. The *miniCTA* has a low pass filter of 10 kHz that limits the highest frequency of the acquired signal, and is used to prevent aliasing in the acquired data. With reference to Figure 2, air velocity profiles were measured at the half depth of the diffuser (in the out-of-plane z direction), at seven different x coordinates. The spacing in the x direction was chosen after preliminary measurements used to evaluate the variation of the mean velocity along the diffuser axis. The distance between profile points in the y direction was 1 mm, which corresponded to one turn of the lead screw. Each profile ended 2 mm from the diffuser walls, in order to exclude the effect of the boundary layer from the analysis.

Hot-wire anemometry data analysis

Amplitude-domain analysis of a random signal, such as the velocity history of a turbulent flow, provides information about the amplitude of the air flow velocity with no time-history information. Hot-wire anemometry produces a record of digitally acquired velocity data

$$\{u\} = \{u_1, \ldots, u_m, \ldots, u_N\} \qquad (4)$$

where each sample m is related to the corresponding time instant t by $t = m\Delta t$. The time interval between samples is given by

$$\Delta t = 1/SR = T/N \qquad (5)$$

where SR is the sampling rate, T the total sampling time, and N the number of recorded samples. In amplitude-domain statistics, the time interval must be large enough to obtain samples that are statistically independent [16]. It is assumed that two velocity samples of a turbulent air flow are uncorrelated when the time interval is equal to two times the integral time scale T_I, which depends on the experimental configuration and the characteristics of the air flow.

When an estimate of T_I is not available from the literature, the autocorrelation function of a single velocity time-history record

$$R_u(\tau) = \lim_{T\to\infty} \frac{1}{T} \int_0^T u(t)\, u(t+\tau)\, \mathrm{d}t \qquad (6)$$

can be used to estimate the integral time scale with a good level of accuracy. In this case T_I can be calculated from [16]

$$T_I = \int_0^\infty \frac{R_u(\tau)}{R_u(0)}\, \mathrm{d}\tau \qquad (7)$$

and the optimum sampling rate for time averaged values is $SR = 1/2\,T_I$.

Frequency-domain analysis refers to the energy spectrum of turbulence, that is the measure of the kinetic energy per unit of mass contained in the frequency interval between f and $f + \mathrm{d}f$. Given a velocity data record $\{u\}$ with total time length T, the energy spectrum is computed through the ensemble-averaged autospectral density function [16]

$$G_u(f) = \frac{2}{n_d\, T} \sum_{k=1}^{n_d} |U_k(f)|^2 \qquad (8)$$

where $U_k(f)$ represents the Fourier transform of the kth sub-

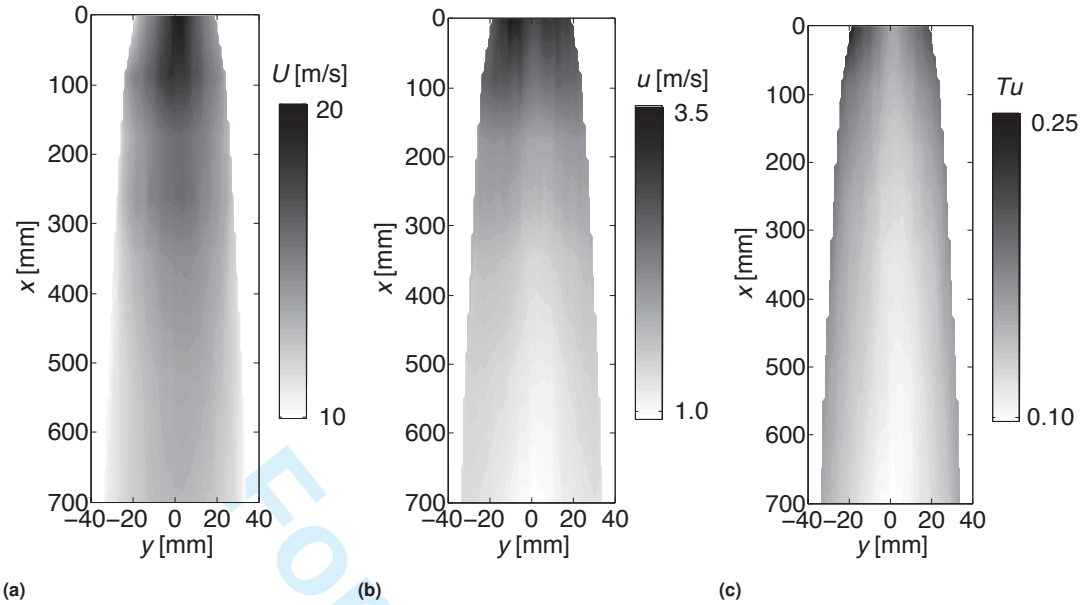

Figure 3. Time-averaged quantities measured in the diffuser: (a) mean velocity U, (b) rms fluctuating velocity u, and (c) turbulent intensity Tu.

record of $\{u\}_k$, with total length $T_k = T/n_d$.

Air flow results

Air velocity data used to characterise the mean air velocity U and the rms fluctuating velocity u were acquired using a sampling rate of 200 Hz according to the procedure described in the previous section. Figure 3 shows the contour plots of the stream-wise mean velocity (a), the rms fluctuating velocity (b) and the turbulence intensity (c), which were obtained by linear interpolation of the single measured profiles. The asymmetry of the plots confirms that the flow is unsteady and not fully developed, and in turn the need of an experimental approach.

The plots show that the mean velocity is maximum at the centre of the diffuser and its values decreases from 20 m/s at the top of the diffuser to 13 m/s at the outlet. On the other hand, the turbulent intensity is maximum next to the walls and range from 0.25 at the inlet to 0.17 at the outlet. However, since in this study a fibre is allowed to oscillate around the axis of the diffuser, it is worth noting that the turbulence intensity at the centre of the diffuser decreases from 0.17 at the top to 0.10 at the end section. This configuration shares features with the flow field in a conventional diffuser[11], as well as in a free jet[22]. The mean velocity profile in a conical diffuser is uniform at the inlet and, due to the adverse pressure gradient, has a maximum that becomes progressively more pronounced in the stream-wise direction. In a free jet the velocity is maximum at the nozzle and then progressively decreases away from the nozzle. The peak of turbulent intensity in a conical diffuser is next to the walls at the inlet, with a magnitude that progressively increases in the stream-wise direction, and a peak that moves towards the diffuser axis. In a free jet the turbulent intensity is maximum at the inlet, next to nozzle radius, and progressively decreases away from the nozzle, while its profile becomes more uniform.

Data series for the frequency-domain analysis were acquired at the centre of the profiles $x = 0, 175, 350, 525, 700$ mm. The sampling rate of 20 kHz was two times the cut-off frequency, according to the Nyquist theorem[23]. At the centre of each profile the integral time T_I was evaluated using Equation 7, while the integral length was calculated using Taylor's hypothesis[21] $L_T = U_c T_I$, where U_c is the mean velocity at the centre of each profile. Figure 4 shows the variation of T_I and L_T along the diffuser.

Figure 5 shows the energy spectra of turbulence evaluated through the autospectral density function defined by Equation 8, after the smoothing of $G_u(f)$. The energy spectrum is related to the rms fluctuating velocity u by

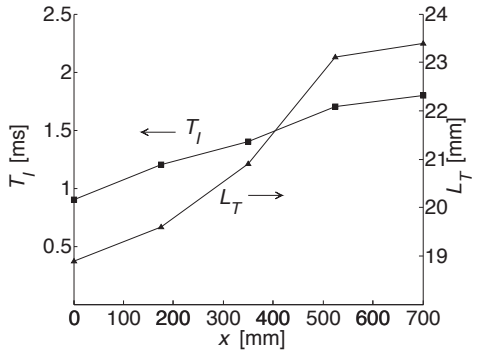

Figure 4. Variation of integral time T_I and integral length L_T of turbulence along the diffuser.

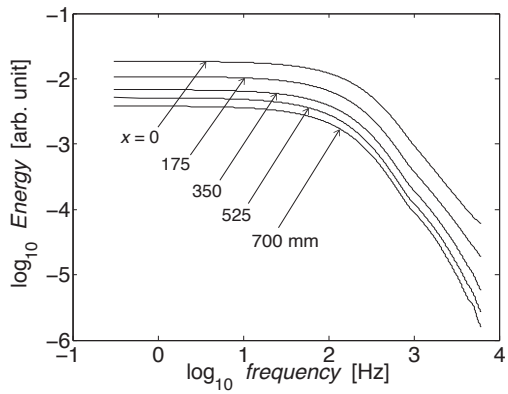

Figure 5. Turbulence energy spectra measured at the centre of the profiles at locations $x = 0,\ 175,\ 350,\ 525,$ and 700 mm along the diffuser axis.

Parseval's theorem

$$u^2 = \int_0^\infty G_u(f)\mathrm{d}f \tag{9}$$

As can be observed from the spectra, the energy in the diffuser decreases from the inlet towards the outlet. Such a result is in agreement with the variation of the fluctuating velocity presented in Figure 3b which shows that, although u and the energy spectra are obtained independently, u also decreases downstream in the diffuser.

The plateau present in all the spectra at low frequency corresponds to the energy-containing range of the spectrum, which is related to the kinetic energy of the large scale eddies. The energy-containing range, which contains the bulk of the total turbulent energy[18], plays the major role in the fibre dynamics, and its identification is required to model accurately the fibre-flow interaction. In addition, the upper frequency limit of the energy-containing range gives information about the highest frequency of the energy-containing eddies. Figure 5 shows that the upper frequency limit decreases from 200 Hz to 50 Hz from the inlet to the outlet section. This result is in agreement with the integral time plot of Figure 4, where T_I increases in the stream-wise direction.

Motion of a single fibre and a single filament in the diffuser

The rig has two Perspex walls that allow visualisation of the fibres during the spunbonding trials. In this section we investigate the displacement of a single fibre under the air flow described in the previous section. Due to the small diameter of a spunbonding fibre, which is typically in the range 20-70 μm, as well as the reflectivity of the walls and marks present on the outer surface of the wall (see Figure 7), it was not possible to obtain clear images of a single spunbonding fibre through the Perspex walls. To overcome this problem, a commercial nylon filament with diameter 200 μm was visualised within the diffuser, while a single spunbonding fibre was visualised only outside the diffuser, at the outlet section.

Experimental equipment and procedure

The displacement of the filament was visualised through the Perspex walls using a Casio EX-FH20 digital camera, with the experimental setup shown in Figure 6. The filament was attached at one end to a metallic wire with diameter 1 mm, which in turn was fastened to the bottom plates of the secondary air duct. While the interaction between the main flow and the supporting wire can be expected to increase locally the turbulence intensity, considering the small diameter of the wire and the significant level of turbulence intensity already present at the top of the diffuser, this effect can be neglected. The camera was placed at different positions along the x axis, by using an adjustable arm fixed to the Perspex wall. Black cardboard was placed behind the rear wall to enhance the image background. Pictures of the filament in motion were taken in the $x-y$ plane at five different sections: 168, 371, 548, 769, and 1000 mm along the x axis. For each section a sequence of 40 frames was recorded, with a time interval of 25 ms between frames.

As a rule of thumb, to obtain a clear profile of the filament in motion it is important firstly to use a light exposure which is short enough to avoid blurred images, and secondly to compensate for the reduction of light by maximizing the lens opening. However, if the velocity is too high the required exposure time might be so short that the images are too dark and the object cannot be identified. In this case an additional source of light is necessary. In this experiment the best setting in the camera was obtained by using a shutter speed of 1/400, a lens opening at the maximum level of f/2.8, and an ISO speed that varied from 400 to 800. A non-flicker high intensity light (Bowens Studio Lite SL455) was placed approximately 30 cm above the camera, as shown in Figure 6, while the camera was placed at a distance of $10-15$ cm from the wall. The intensity and the position of the light were adjusted in order to reduce the light reflected by the wall.

The air flow setting was as in the previous section. However,

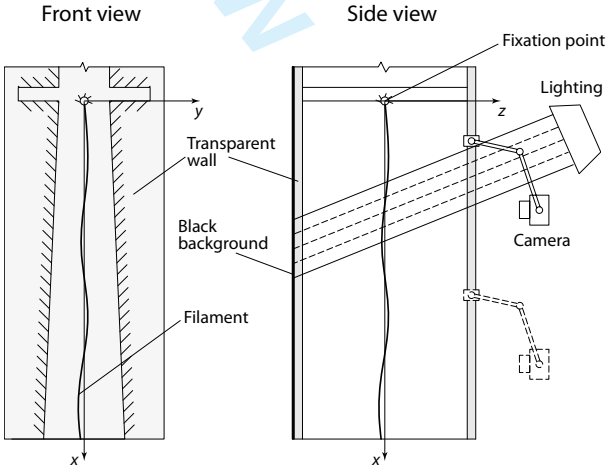

Figure 6. Schematic of the filament and fibre imaging experiment.

since this experiment was undertaken some time after the air flow measurement, the consistency of the air flow field was verified by measuring the mean velocity at the centre of the diffuser outlet. The measured value in this case was 13 m/s which corresponds to the value showed in Figure 3. The nylon filament was taken from a reel of commercial nylon thread for sewing. Before the experiment, waviness of the filament was eliminated by applying a small tensile load under a stream of warm air. Both the filament and fibre lengths were equal to that of the diffuser, i.e. 1 metre.

Single filament results

For each section along the diffuser a sequence of raw images

$$\mathcal{P}_x = \{p_1, \ldots, p_k, \ldots, p_N\}, \quad N = 40 \tag{10}$$

was obtained. Due to the small filament diameter, the quality of the wall surface, and the reflected light, it is difficult to identify clearly the filament in the raw pictures (see Figure 7). This problem was solved by digital image processing in Matlab. Images of $\mathcal{P}_x$ were first converted to grey scale, then the background was eliminated by creating a new set

$$\mathcal{Q}_x = \{q_1, \ldots, q_k, \ldots, q_{N-1}\} \tag{11}$$

where each image is obtained from the elements in $\mathcal{P}_x$ by subtracting from the frame taken at the next time instant t_{i+1}, the frame at the current time instant t_i, that is

$$q_k = p_{k+1} - p_k, \quad k = 1, \ldots, N-1 \tag{12}$$

In this way light reflections and marks were eliminated. The contrast in each image of $\mathcal{P}_x$ was then increased by using an adaptive histogram equalization technique and, finally, a median filter was used to improve the filament definition [19]. Figures 7a and 7b show an example of raw images at the previous time instant p_k and at the next time instant p_{k+1}, acquired at 168 mm below the secondary air inlet. The position of the filament can hardly be recognized by the naked eye. Figure 7c shows the corresponding enhanced image q_k. The location of the filament at a given height x can be identified by the position of the intensity peak of the pixels. A time series of the filament positions $\mathcal{Y}_x = \{y_1, y-2, \ldots, y_{N-1}\}$ was extracted at each section, and the amplitude of oscillation was characterized through the standard deviation of the filament positions. The amplitude of oscillation increases monotonically towards the diffuser outlet until a maximum of about 7 mm, as shown in Figure 8. Here the error bars are calculated by considering that the standard deviation follows a chi-squared distribution [20], and represent the confidence intervals corresponding to a probability of 98%.

Single fibre results

The same experiment as described above for a nylon filament was also undertaken using a single spunbonding fibre with diameter 18 μm. This time the thinness of the fibre prevented visualisation through the Perspex wall and pictures were taken only for the small portion of fibre outside the diffuser outlet. Figures 10a and 10b show two successive frames. Even outside the diffuser the fibre position can barely be recognized by the naked eye. A significant improvement

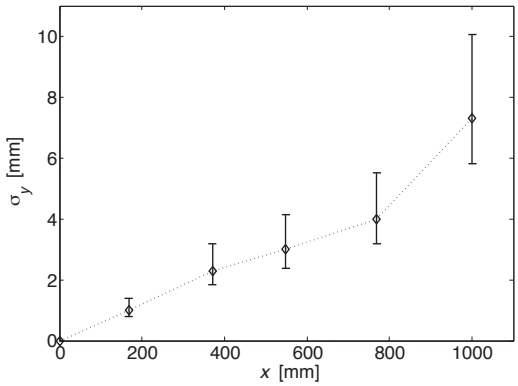

Figure 8. Standard deviation σ_y of the filament position in the y direction as a function of the position x along the diffuser. The error bars represent the confidence intervals corresponding to a probability of 98%.

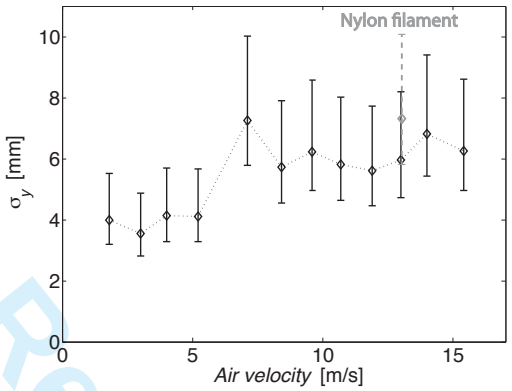

Figure 9. Standard deviation σ_y of the position of the 18 μm fibre end point in the y direction as a function of the mean velocity measured at the diffuser outlet. The error bars represent the confidence intervals corresponding to a probability of 98%.

was obtained after applying the image processing technique described above, as shown in Figure 10c. The effect of varying the primary air flow on the fibre oscillation is presented in Figure 9, which shows the standard deviation of the fibre position as a function of the mean air flow velocity, both measured at the centre of the diffuser outlet. Increasing the air velocity from about 2 m/s to about 15 m/s increases the fibre oscillation from 2 mm to 4 mm.

In the same figure it is shown that under the same air flow rate the standard deviation of the thicker filament is larger than that of the fibre (data in light grey). It is expected that an increase of fibre diameter has two effects on the amplitude of oscillation: the amplitude can either grow, due to a larger exposed area which leads to higher air drag forces, or decrease, due to the growing fibre inertia and bending stiffness, depending on which phenomenon plays the dominant role. Since the experiment does not provide enough information to identify the dominant term, this topic

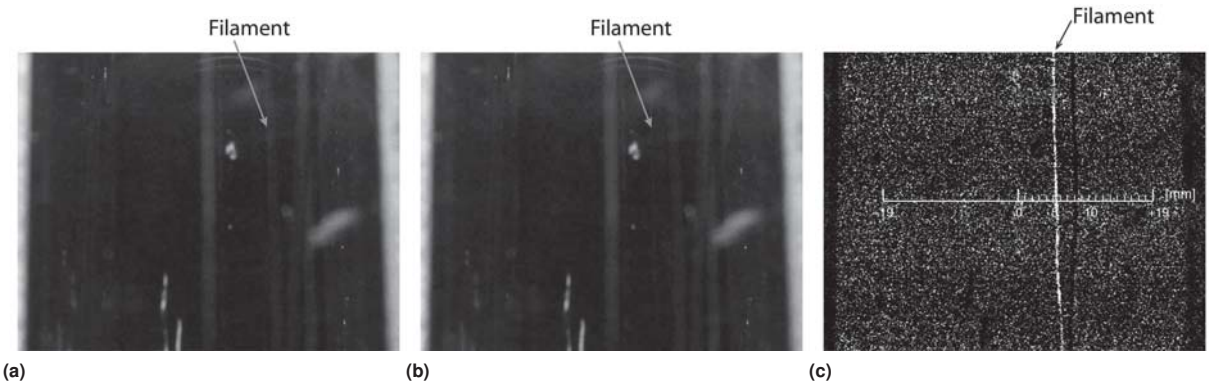

Figure 7. Examples of filament frames at $x = 168$ mm. (a) Raw image p_i at time t_i, (b) raw image p_{i+1} at time t_{i+1}, and (c) image q_i at time t_{i+1} after image processing.

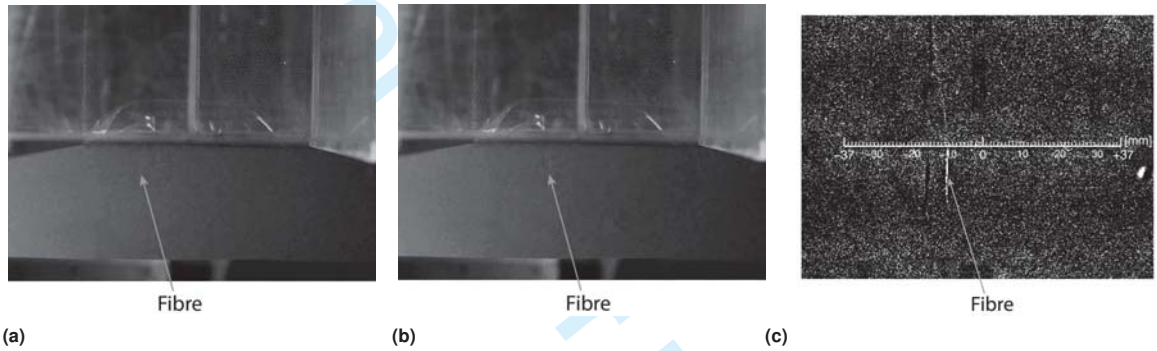

Figure 10. Examples of fibre frames at the diffuser outlet. (a) Raw image at time t_i, (b) raw image at time t_{i+1}, and (c) image at time t_{i+1} after image processing.

will be discusses in more detail using the model described in the companion paper, Part II.

Concluding discussion

Studying the fibre-turbulent flow interaction is a fundamental step for the understanding of the fibre deposition and the formation of the fibre web in nonwovens produced by the spunbonding process. A turbulent air flow develops within the diffuser as a result of the interaction between the primary and the secondary air flow, under the effect of a negative pressure gradient which decreases the air flow velocity and increases turbulence. The turbulent air stream is highly turbulent at the top of the diffuser, with a turbulent intensity larger than 0.25, and moderately turbulent with a turbulent intensity of 0.10 at the outlet. The length scale of turbulence, which in the spun-bonding process represents an estimate for the length scale of the fibre-flow interaction, increases from 19 mm to 23 mm downstream the diffuser. A similar behaviour is observed for the cut-off frequency of the energy containing range of the energy spectrum, which decreases from 200 Hz to 50 Hz from the inlet to the outlet of the diffuser.

Under these conditions a nylon filament with cross-section diameter 200 μm oscillates with a maximum amplitude of oscillation of 7.5 mm at the diffuser outlet, whereas a spun-bonding fibre has a maximum amplitude of 6 mm. It is observed also that the amplitude of oscillation of a single fibre increases by increasing the air flow velocity.

The characterisation of the fibre-air flow interaction in the spun-bonding process presented here is a fundamental step which is necessary to obtain realistic air flow and fibre amplitude data. This in turn is a prerequisite to modelling the fibre architecture in the spun-bonding process, and better understanding the effect of process conditions on mechanical performance. However, an experimental study of the motion of fibres in the spun-bonding process can only provide limited information due to the large number of variables that are involved, and the complexity of this phenomenon. For example in a spun-bonding rig, by varying the main air flow rate the mean velocity U in the diffuser is varied together with the fluctuating velocity u, so that the influence of the individual parameters cannot be understood.

To overcome this limitation in the companion paper, Part II, we develop a mathematical model, which is able to describe the behaviour of the fibre as a function of the fibre diameter and air flow parameters such as mean velocity, fluctuating velocity, turbulence length scale, and turbulence energy spectrum. The model will be used to extend the experimental investigation that has been presented here to

arbitrary turbulent air flows to predict the fibre motion before deposition.

Acknowledgements

The authors are grateful to Fitesa Germany GmbH for the financial support.

References

1. Beyreuther R and Brunig H. *Dynamics of fibre formation and processing*. Berlin: Springer, 2010.
2. Bhat G S and Malkan S R. Extruded continuous filament nonwovens: Advances in scientific aspects. *J Appl Polym Sci* 2002; 83(3):572–585.
3. Matsui M. Air drag on a continuous filament in melt spinning. *T Soc Rheo* 1976; 20(3):465–473.
4. Hearle J W S, and Sultan M A I and Govender S. Form taken by threads laid on a moving belt - I. Experimental study. *J Text I* 1976; 67(11):373–376.
5. Hearle J W S, and Sultan M A I and Govender S. Form taken by threads laid on a moving belt - II. Mechanisms and theory. *J Text I* 1976; 67(11):377–381.
6. Hearle J W S and Sultan M A I and Govender S. Form taken by threads laid on a moving belt - III. Comparison of materials. *J Text I* 1976; 67(11):382–386.
7. Rao R S, and Shambaugh R L. Vibration and stability in the melt blowing process. *Ind Eng Chem* 1993; 32(12):3100–3111.
8. Marla V T and Shambaugh R L. Three-dimensional model of the melt-blowing process. *Ind Eng Chem* 2003; 42(26):6993–7005.
9. Bo Z. Experimental study and numerical analysis for prediction of the fibre diameter of polylactic acid (PLA) spunbonded nonwovens. *Fibres Text East Eur* 2009; 76(5):82–86.
10. Marheineke N and Wegener R. Modeling and application of a stochastic drag for fibers in turbulent flows. *Int J Multiphas Flow* 2011; 37(2):136–148.
11. Okwuobi P A C and Azad R S. Turbulence in a conical diffuser with fully developed flow at entry. *J Fluid Mech* 1973; 57(3):603–622.
12. Wu T T and Shambaugh R L. Characterization of the melt blowing process with laser doppler velocimetry. *Ind Eng Chem* 1992; 31(1):379–389.
13. Beard J H and Shambaugh R L and Shambaugh B R and Schmidtke D W. On-line measurement of fibre motion during melt blowing. *Ind Eng Chem* 2007; 46(22):7340–7352.
14. Davidson P A (2004) *Turbulence. An introduction for Scientists and Engineers*. Oxford University Press.
15. White F M (2001) *Fluid Mechanics*. McGraw-Hill.
16. Bruun H H (1995) *Hot-Wire Anemometry, Principles and Signal Analysis*. Oxford University Press.
17. Jorgensen E F (2002) *How to measure turbulence with hot-wire anemometers. A practical guide*. DANTEC Dynamics.
18. Pope S B (2000) *Turbulent Flows*. Cambridge University Press.
19. Gonzales R C and Woods R E and Eddins S L (2009) *Digital image processing using MATLAB*. Gatesmark Publishing.
20. Ross S (1998) *A first course in probability*. Prentice-Hall International.
21. Taylor G I The spectrum of turbulence. *Proc R Soc A* 1938; 164:479–490.
22. Ball C G and Fellouah H and Pollard A. The flow field in turbulent round free jets. *Progr in Aerosp Sci* 2012; 50:1–26.
23. Oppenheim A V (1999) *Discrete-time signal processing*. Prentice Hall.